J. Indian Chem. Soc.,
Vol. 92, December 2015, pp. 1939-1947

Forced ether oxygen coordination from reduced Schiff base ligand in [Cu_2] complexes : Synthetic preference, trapping of carboxylates and catechol oxidation†

Tufan Singha Mahapatra, Krishna Chattopadhyay, Dipmalya Basak, Manisha Das, Avik Bhanja, Mousumi Biswas and Debashis Ray*

Department of Chemistry, Indian Institute of Technology, Kharagpur-721 302, West Bengal, India

E-mail : dray@chem.iitkgp.ernet.in *Fax* : 91-3222-82252

Abstract : Phenol-centered heptadentate ligand H_5L bearing two adjacent and flexible amine-ether-alcohol arms enforced ether oxygen coordination in $[Cu_2(\mu\text{-}H_4L^2)_2](CH_3CO_2)_2$ (1) and $[Cu_2(\mu\text{-}H_4L^2)_2](HCO_2)_2$ (2). Dangling ligands arms were used to entrap carboxylate anions. Probable high nuclearity [Cu_4] complexes were not formed due to the removal of acetate and formate anions from the first coordination sphere. Coordination of ether oxygen in *apical* position was possible due to enhanced flexibility of the ligand arms through imine reduction. X-Ray structure determination and analysis of Hirshfeld surfaces indicated the synergistic role of crystal packing and hydrogen bonding interaction for supramolecular trapping of carboxylates. Functional behavior in MeOH : MeCN (1 : 10) medium showed that complex 1 is more efficient than complex 2 for catechol oxidation.

Keywords : [Cu_2] complex, Schiff base ligand, oxidation, trapping.

Introduction

During the last three decades, the synthesis, characterization and rationalization of binucleating ligand bound [Cu_2] complexes have received significant interest due to their involvement as model compounds in magnetic-exchange interaction[1], DNA binding and cleavage[2], oxidation of catechols[3,1d] and as building units for the construction of tetra- and pentanuclear complexes[4]. These ligands having two coordination pockets suitable for providing strong and highly directional metal-ligand interactions that can lead to [Cu_2L] and [Cu_2L_2] species depending upon the availability of co-ligands for stabilization of different types of molecular entities. Thus coordination of solvent water and added metal salt derived HO^-, O_2^-, RCO_2^- and NO_3^- groups as well as CO_3^{2-} group from fixation of atmospheric CO_2 are crucial along with binding of organic phenol bearing ligand with two adjacent ligand donor arms[5]. The tendency of the Cu^{II} ions in these pockets to accept a fifth coordinating group in the *apical* position is also important at the same time. Thus competitive binding of HO^-, O^{2-}, RCO_2^- and NO_3^- groups as ancillary ligand usually trigger the assembly of [Cu_2L] units around HO^-, O_2^- and NO_3^- groups during the formation of [Cu_4] and [Cu_{12}] aggregates[4a-b,6]. Rigid azomethine (-CH=N-) fragments play important role for such assembly processes. In an attempt to realize the role of flexible and long ligand side arms in satisfying copper coordination environments we examined the reactivity of reduced Schiff base ligand with two different metal salts under chosen reaction conditions to provide nucleating groups like HO^- and O^{2-}.

In this regard the type of ligand is important in stabilizing the [Cu_2] complexes and for better understanding of substrate binding and bimetallic catalysis. Recent studies have indicated that phenoxido bridged [Cu_2] complexes can function as useful chemical model for catecholase enzyme[7–10]. A Cu···Cu separation in the range of 2.9–3.2 Å is ideal for binding of substrate catechol by two metal ion centers[11a]. It is reported in some cases that double-phenoxido or -hydroxido bridges give catalytically

†**In honour of Professor Animesh Chakravorty on the occasion of his 80th birth anniversary.**

inactive species[11b] although other similar double-bridged compounds have shown good catalytic activity[11c-g].

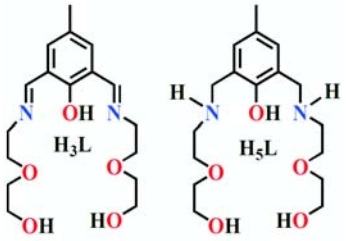

Chart 1. H_3L and H_5L.

In trying to study and isolate the reaction products of $Cu(RCO_2)_2 \cdot H_2O$ (R = Me and H) with ligand 2,6-bis[((2-(2-hydroxyethoxy)ethyl)amino)methyl]-4-methylphenol (H_5L) (Chart 1) we examined the competitive binding capacity of the reduced and flexible ligand arms and available ancillary groups in stabilizing the $[Cu_2]$ complexes as against other higher order aggregates. The precursor ligand H_3L (Chart 1) was used by Oshio *et al*. for the generation of a hexanuclear family of $[Mn_4Ln_2]$ complexes[12]. Herein, two new $[Cu_2]$ complexes $Cu_2(\mu\text{-}H_4L)_2](CH_3CO_2)_2$ **(1)** and $Cu_2(\mu\text{-}H_4L)_2](HCO_2)_2$ **(2)** of H_4L^- have been isolated and crystallographically characterized. Along with spectroscopic characterization solution phase catalytic activity for catechol oxidation have also been examined.

Experimental

Starting materials : The chemicals were used as obtained from the following sources : copper(II) acetate, copper(II) carbonate, formic acid and triethylamine from E. Merck (India) and 2-(2-aminoethoxy)-ethanol from Alfa Aesar. All other chemicals and solvents were reagent grade and used as received without further purification. 2,6-Diformyl-4-methylphenol was prepared following a literature procedure[13]. $Cu(HCO_2)_2 \cdot 4H_2O$ was synthesized by adding copper(II) carbonate to a solution of formic acid (20 mL, 98–100%) in 20 mL of water with constant stirring until effervescence ceased. Then the solution was filtered, and the clear filtrate was kept on a water bath until deep blue solid of $Cu(HCO_2)_2 \cdot 4H_2O$ separated. The solution was then cooled to room temperature and the separated $Cu(HCO_2)_2 \cdot 4H_2O$ was filtered through suction and dried in vacuum. All manipulations were performed in air.

Synthesis :

H_5L : 2-(2-Aminoethoxy)-ethanol (1 mL, 1.051 g, 10 mmol) was added dropwise to a solution of 2,6-diformyl-4-methylphenol (0.820 g, 5 mmol) in MeOH (40 mL) at ambient temperature and the mixture was stirred for 15 min. The reaction mixture was then refluxed for 2 h and solvent was removed under vacuum to give an oily residue. To an orange MeOH solution (20 mL) of H_3L (1.690 g, 5.00 mmol), $NaBH_4$ (0.38 g, 10 mmol) was added slowly with stirring at 0 °C. The solution was stirred for 2 h at room temperature till colorless and acidified with conc. HCl (3 mL). The reaction mixture was evaporated to dryness followed by extraction with MeOH[14]. The MeOH extract was then evaporated, leaving the product as light yellow viscous oil. Yield : 1.56 g (91%). ^1H NMR ($CDCl_3$, ppm) : δ 6.75 (2H, s, ArH), 4.61 (2H, s(br), NH), 3.79 (4H, s, CH_2), 3.62 (4H, d, CH_2), 3.55 (4H, t, CH_2), 3.49 (4H, t, CH_2), 2.77 (4H, t, CH_2), 2.16 (3H, s, CH_3); ^{13}C NMR ($CDCl_3$, ppm) : δ 154.48, 129.21, 127.83, 124.22, 72.69, 69.82, 61.63, 50.84, 48.33, 20.63.

Synthesis of complexes $[Cu_2(\mu\text{-}H_4L)_2](MeCO_2)_2$ **(1)** : To a colorless solution (10 mL) of H_5L (0.342 g, 1.00 mmol) a methanol solution of $Cu(MeCO_2)_2 \cdot H_2O$ (0.400 g, 2 mmol) was added slowly followed by NEt_3 (0.140 mL, 0.101 g, 1.00 mmol) and stirred for 3 h at room temperature. The reaction mixture was evaporated to give a green solid product and it was washed with cold methanol and dried under vacuum over P_4O_{10}. The solid was dissolved in a minimum quantity of CH_2Cl_2 and an equivalent amount of MeCN was added. Green prismatic single crystals suitable for X-ray analysis were obtained after keeping the solution at room temperature for about 4 days. Yield : 0.650 g, 70%. Anal. Calcd. for $C_{38}H_{76}Cu_2N_4O_{14}$ (940.13 g mol^{-1}) : C, 48.55; H, 8.15; N, 5.96. Found : C, 48.64; H, 8.17; N, 6.04. Selected IR peaks : (KBr, cm^{-1}, vs = very strong, br = broad, s = strong, m = medium, w = weak) : 3400 (br), 3273 (s), 3170 (s), 1576 (vs), 1476 (s), 1400 (m), 1270 (m), 1236 (m); Λ_M (Molar conductivity) : (MeOH solution) 155 Ω^{-1} cm^2 mol^{-1}; UV-Vis : λ_{max}, nm (ε, M^{-1} cm^{-1})] (MeOH) = 592 (161), 353 (4900), 242 (45300).

$Cu_2(\mu\text{-}H_4L)_2](HCO_2)_2$ **(2)** : Complex **2** was obtained following a similar procedure as outlined above for the

synthesis of **1** by using $Cu(HCO_2)_2{\cdot}4H_2O$ (0.450 g, 2 mmol) in place of $Cu(CH_3CO_2)_2{\cdot}H_2O$. Yield : 0.575 g, 64%. Anal. Calcd. for $C_{36}H_{56}Cu_2N_4O_{14}$ (895.95 g mol^{-1}) : C, 48.26; H, 6.30; N, 6.25. Found : C, 48.31; H, 6.26; N, 6.11. Selected IR peaks : (KBr, cm^{-1}, vs = very strong, br = broad, s = strong, m = medium, w = weak) : 3400 (br), 3297 (s), 3182 (s), 1591 (vs), 1474 (s), 1335 (m), 1270 (m), 1237 (m); Λ_M (Molar conductivity) : (MeOH solution) 165 Ω^{-1} cm^2 mol^{-1}; UV-Vis spectra [λ_{max}, nm (ε, L mol^{-1} cm^{-1})] : (MeOH solution) = 592 (165), 353 (2700), 241 (24800).

Physical measurements : The elemental analyses (C, H and N) were performed with a Perkin-Elmer model 240C elemental analyzer. Fourier transform infrared (FT-IR) spectra in KBr (4000–400 cm^{-1}) were recorded on a Perkin-Elmer 883 spectrometer. Solution electrical conductivity and electronic spectra were obtained using a Unitech type U131C digital conductivity meter with a solute concentration of about 10^{-3} *M* and a Shimadzu UV 3100 UV-Vis-NIR spectrophotometer, respectively. The purity of powder complexes for all three samples were determined by PXRD using a BRUKER AXS X-ray diffractrometer (40 kV, 20 mA) using Cu Kα radiation (k = 1.5418 Å) over the 5–50° (2θ) angular range and a fixed-time counting of 4 s at 25 °C.

Computational method : Hirshfeld surfaces were mapped using Crystal Explorer (version 3.1) software using the crystal structure coordinates of CIF files[15]. Graphical plots of the molecular Hirshfeld surfaces were mapped with normalized contact distance (d_{norm}) using a color code of red-white-blue, where red spots indicate shorter contacts, white regions highlights contacts around the van der Waals distance, and the blue areas are for longer contacts.

X-Ray crystallography : X-Ray diffraction analysis was performed on suitable single crystals of **1** and **2.** Intensity data were collected on a Bruker SMART APEX-II CCD diffractometer, equipped with a fine focus 1.75 kW sealed tube Mo Kα radiation (α = 0.71073 Å), with increasing ω (width of 0.3° per frame) at a scan speed of 5 s per frame at 293 K. The SMART software was used for data acquisition. Data integration and reduction were performed with SAINT and XPREP software[16]. Multiscan empirical absorption corrections were applied to the data using the program SADABS[17]. Structures were solved by direct methods using SHELXS-97[18] and refined with full-matrix least squares on F^2 using the SHELXL-97[19] program package incorporated into WinGX 1.80.05[20]. The locations of the heaviest atoms (Cu) were easily determined, and the O, N, and C atoms were subsequently determined from the difference Fourier maps. All non-hydrogen atoms were refined anisotropically. The H atoms were introduced in calculated positions and refined with fixed geometry and riding thermal parameters with respect to their carrier atoms. A summary of the crystal data and relevant refinement parameters are given in Table 1. CCDC 1431950 (**1**) and 1431951 (**2**) contain the supplementary crystallographic data for this paper.

Table 1. Crystal parameters and refinement data for **1** and **2**

Parameters	**1**	**2**
Formula	$C_{38}H_{76}Cu_2N_4O_{14}$	$C_{36}H_{56}Cu_2N_4O_{14}$
F.W. (g mol^{-1})	940.13	895.95
Crystal system	Triclinic	Triclinic
Space group	$P\bar{1}$	$P\bar{1}$
Crystal color	Green	Green
Crystal size (mm^3)	0.33 × 0.27 × 0.24	0.32 × 0.28 × 0.22
a (Å)	9.9101(9)	9.863(3)
b (Å)	10.3296(9)	9.870(3)
c (Å)	11.1834(10)	11.279(3)
α (deg)	103.891(3)	94.383(9)
β (deg)	94.977(3)	105.763(8)
γ (deg)	101.130(3)	104.233(8)
V ($Å^3$)	1079.73(17)	1012.1(5)
Z	1	1
D_c (g cm^{-3})	1.445	1.470
μ (mm^{-1})	1.054	1.121
F(000)	502	470
T (K)	298(2)	293(2)
Total reflections	13954	11525
R(int)	0.0378	0.0727
Unique reflections	4342	3501
Observed reflections	3411	2629
Parameters	262	253
R_1; wR_2 ($I > 2\sigma(I)$)	0.0511, 0.0972	0.0698, 0.1938
GOF (F^2)	2.265	1.103
Largest diff peak and hole (e $Å^{-3}$)	0.842, –0.649	0.977, –1.108
CCDC No.	1431950	1431951

Results and discussion

Synthesis : The azomethine (-CH=N-) fragments bearing Schiff base H_3L (2,6-bis[((2-(2-hydroxyethoxy)ethyl)-imino)methyl]-4-methylphenol) was synthesized by the condensation of 4-methyl-2,6-diformylphenol and 2-(2-aminoethoxy)-ethanol in about 95% yield. $NaBH_4$ reduction next provided H_5L (2,6-bis[((2-(2-hydroxyethoxy)-ethyl)amino)methyl]-4-methylphenol (Scheme 1). Reaction of H_5L with $Cu(RCO_2)_2{\cdot}H_2O$ (R = CH_3, H) and NEt_3 in 1 : 2 : 1 molar ratio in MeOH provided two $[Cu_2]$ species **1** and **2** as green solid in moderate yield under ambient condition. In presence of carboxylates and water derived HO^- and O^{2-} ions no *dimer-of-dimer* assembly for $[Cu_4(OH)_2]$ or $[Cu_4O]$ species took place (Scheme 1, left). Increased ligand arm flexibility of reduced H_5L, facilitated by $-CH_2$-NH- moieties, resulted in axial coordination of ether oxygen atom from one half of the ligand (Scheme 1, right). Eq. (1) summarizes the formation of **1** and **2** from the employed reaction conditions.

$$2H_5L + 2Cu(RCO_2)_2{\cdot}H_2O + 2NEt_3 \longrightarrow [Cu_2(\mu\text{-}H_4L)_2](RCO_2)_2 + 2(NHEt_3)(RCO_2) + 2H_2O \quad (1)$$

Prior to molecular structure determination elemental analysis and molar conductivity studies establish the above proposed formula for **1** and **2**.

Spectral characterizations :

FT-IR spectra :

Two bound H_4L^- ligands in complexes **1** and **2** can be identified from their NH stretching vibrations (ν_{NH}) at 3170 and 3182 cm^{-1} respectively (Fig. S1). In absence of any water of crystallization the ν_{OH} for hydrogen bonded terminal hydroxyl groups of the ether-alcohol arms were identified at 3273 cm^{-1} and 3297 cm^{-1} respectively, along with broad shoulders around 3400 cm^{-1}. The presence of two different carboxylate groups as counter anions register $\nu_{as(COO)}$ and $\nu_{s(COO)}$ bands at 1576 cm^{-1} and 1236 cm^{-1} in **1** and at 1591 cm^{-1} and 1237 cm^{-1} in **2**. These values and their differences ($\Delta\nu = \nu_{as(COO)} - \nu_{s(COO)}$) in the order of 340 cm^{-1} and 354 cm^{-1} respectively, for **1** and **2** clearly indicate their presence as non coordinating anions trapped in the crystal lattice.

Electronic spectra :

Electronic absorption spectral change in MeOH during metal ion coordination and formation of complexes **1** and **2** are presented in Fig. S2. Presence of Cu^{II} ions are clearly discernible by identifying absorption bands in MeOH at 592 nm with molar extinction coefficient values of 161 and 165 L mol^{-1} cm^{-1} for **1** and **2** respectively. Next high energy bands at 353 nm (ε = 4900 and 2700 L mol^{-1} cm^{-1}) were considered for $PhO^- \rightarrow Cu^{II}$ charge transfer transitions within $Cu_2(OPh)_2$ motifs. The characteristic ligand centered π–π^* transition was seen at 287 nm (ε = 2240 L mol^{-1} cm^{-1}). Intra ligand π–π^* transitions were blue shifted to 242 nm (ε = 45300 L mol^{-1} cm^{-1}) and 241 nm (ε = 24800 L mol^{-1} cm^{-1}) for complexes **1** and **2**, respectively.

Powder X-ray diffraction :

For elemental analysis and other solution measurements as synthesized powder samples were utilized. Both FT-IR measurements and the powder XRD technique were very useful to check the phase purity and exactness of the prepared complexes in powdered form in different batch of synthesis. The experimental powder XRD pattern for each complex is consistent with the simulated one obtained from

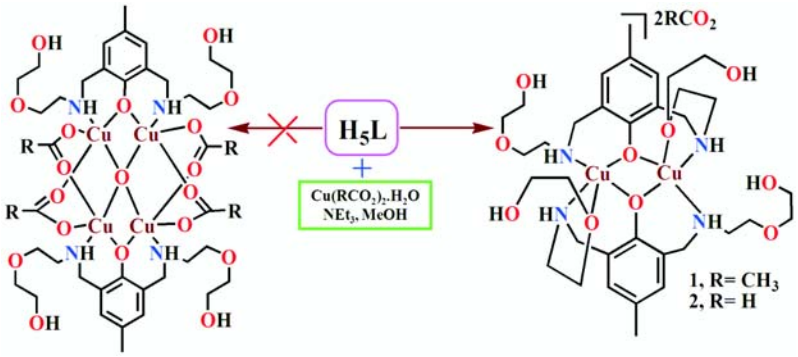

Scheme 1. Schematic representation of hitherto unknown $[Cu_4O]$ and obtained $[Cu_2]$ complexes.

the single crystal X-ray diffraction data (cif files). Most of the peak positions of the simulated and experimental patterns are in good agreement with each other, and slight difference in intensity may be is attributed to the orienta-

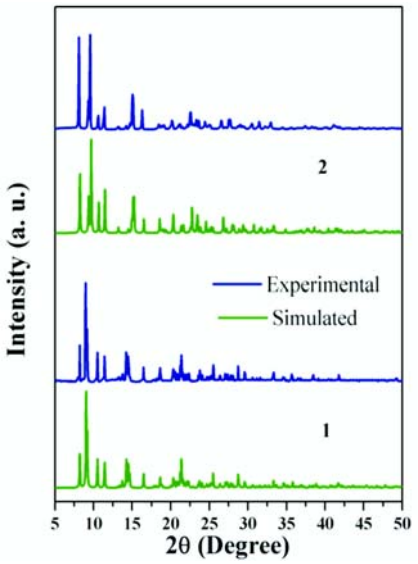

Fig. 1. Experimental (green) and simulated (blue) PXRD patterns for **1** and **2**.

tion of the powder samples (Fig. 1).

Description of crystal structures :

$[Cu_2(\mu\text{-}H_4L)_2](CH_3CO_2)_2$ (**1**) *and $Cu_2(\mu\text{-}H_4L)_2](HCO_2)_2$* (**2**) : Single crystal X-ray diffraction revealed that complexes **1** and **2** crystallizes in triclinic $P\bar{1}$ space group with inversion centers at the midpoint of Cu1···Cu1*. The molecular structures of **1** and **2** are shown in Fig. 2 and selected bond lengths and angles are provided in Table 2. The bound H_4L^- units provide adjacent ONO and NO chelate bites with bridging oxygen from phenoxido group. Two six-membered adjacent bites around the phenoxido unit are highly puckered due to the presence of two adjacent sp^3 hybridized carbon atoms. The chelate ring from bidentate coordination remains in half-chair conformation. The back-to-back square-pyramidal coordination geometry around each Cu atom shows long (2.491 and 2.419 Å) *apical* bonds to ether oxygen atoms. Weak ether oxygen coordination did not lead to any kind of appreciable trigonal distortion as seen from the calculated Addison parameter (τ) values of 0.016 and 0.033, respectively for **1** and **2**. The Cu-O distances within Cu_2O_2 core are very close and range from 1.941–1.954

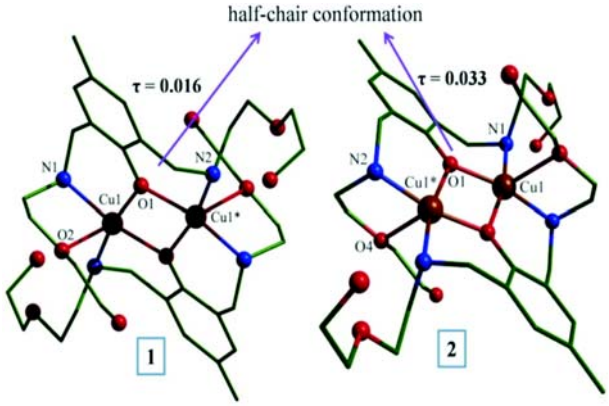

Fig. 2. Perspective view **1** and **2**. The starred atoms represent symmetry code (–x, –y, –z). H atoms are omitted for clarity. Color scheme : Cu, brown; O, red; N, blue; C, green.

Å (Table 2). Generation of -CH_2-NH- units from -C=N- is responsible for the elongation of C-N distances from 1.271–1.285 Å to 1.483–1.503 Å. The Cu-N(amine) bond distances involving sp^3 hybridized nitrogen atoms are longer in 1.984–2.000 Å range and in good agreement

Table 2. Selected interatomic distances (Å) and angles (°) of **1** and **2**

Complex **1**			
Bond distances			
Cu1-O1	1.941(2)	Cu1-N1	1.995(3)
Cu1-O1*	1.954(2)	Cu1-O2	2.491(3)
Cu1-N2*	1.984(3)	Cu1···Cu1*	3.044(2)
Bond angles			
O1-Cu1-O1*	77.23(1)	N2*-Cu1-N1	95.92(1)
O1-Cu1-N2*	167.70(1)	O1-Cu1-O2	91.01(9)
O1*-Cu1-N2*	91.59(1)	O1*-Cu1-O2	109.68(1)
O1-Cu1-N1	94.44(1)	N2*-Cu1-O2	97.67(1)
O1*-Cu1-N1	168.77(1)	N1-Cu1-O2	77.62(1)
Cu1-O1-Cu1*	102.77(1)		
Complex **2**			
Bond distances			
N2*-Cu1	2.000(5)	Cu1-O1	1.945(4)
O4*-Cu1	2.419(4)	Cu1-N1	1.985(5)
Cu1-O1*	1.944(4)	Cu1···Cu1*	3.053(1)
Bond angles			
O1-Cu1-O1*	76.6(1)	N1-Cu1-O4*	98.1(1)
O1*-Cu1-N1	166.6(1)	N2*-Cu1-O4*	79.0(1)
O1-Cu1-N1	91.9(1)	N1-Cu1-N2*	95.8(1)
O1*-Cu1-N2*	94.6(1)	O1*-Cu1-O4*	91.9(1)
O1-Cu1-N2*	168.5(1)	O1-Cu1-O4*	108.2(1)
Cu1-O1-Cu1*	103.4(2)		

with the literature values (~1.977–2.007 Å)[8,9]. The Cu···Cu separation amounts to 3.0437 and 3.0530 Å, for **1** and **2**, respectively, which are close to the separations found in phenoxido-bridged [Cu_4O] complexes[4a,4b].

Unique trapping of carboxylate anions by dangling ether-alcohol arms of the ligands have been established by the intricate hydrogen bonding network. In complex **1**, the O12 of acetato group engage in hydrogen bonding interaction with H3 (O···O, 2.732 Å) of terminal OH groups of ether oxygen coordinated ligand arms. Whereas O11 of acetato oxygen show three hydrogen bonding interactions with H5A attached to O5 (O···O, 2.828 Å) of dangling ligand arms and H1* and H2 from the reduced nitrogen centers N1* and N2 (O···N, 3.018 and 2.956 Å, respectively) (Fig. S3, Table S1). In complex **2**, the O7 and O6 formato group form strong hydrogen bonds with H3 and H10 hydrogen atoms on O3 and O5 of ligand ether-alcohol arms showing O···O separation of 2.780 and 2.708 Å, respectively. The H1 atom on amine N1 also show interaction with formato O7 (O···N, 2.974 Å) (Fig. S3, Table S1). Trapping of acetate anions of complex **1** in space fill model during crystal packing is shown in Fig. S4.

Hirshfeld surfaces :

The analysis of crystal structure data using CrystalExplorer 3.1 provides a visual picture for different types of non-bonding interactions and can be clearly identified by the shapes, contours, and colors[13]. The found surfaces provide insight into the varying inter- and intramolecular interactions. The Hirshfeld surfaces of complex **1** and **2** have been displayed in Fig. 3, showing the surfaces that have been mapped over a d_{norm} range of –0.5 to 1.5 Å. The normalized contact distance (d_{norm}) in the Hirshfeld surface map is defined as [eq. (2)].

$$d_{norm} = [(d_i - r_i^{vdW})/r_i^{vdW}] + [(d_e - r_e^{vdW})/r_e^{vdW}] \quad (2)$$

where d_i and d_e are the distances from the surface to the nearest atom interior and exterior, respectively and r_i^{vdW} and r_e^{vdW} are the van der Waals radii of the nearest atom interior to the surface and exterior to the surface, respectively. The hydrogen bonding interactions (O-H···O and N-H···O) are effectively viewed in the spots with the large deep red circular depressions on the d_{norm} surfaces. The light red spots are due to C-H···O interactions and red to white regions correspond to H···H contacts. The large deep red circular spots visible clearly in **1** and **2** are due to the presence of extensive hydrogen bonding interactions (Fig. 3).

Reactivity of the complexes, Kinetic evaluation for catechol oxidase activity : The catecholase like activity of **1** and **2** was evaluated for oxidation of the prototypical catechol oxidase substrate 3,5-di-tert-butylcatechol (3,5-DTBC) by UV-Vis spectroscopy. Bulky tertiary butyl groups at 3 and 5 positions render low redox potential suitable for oxidation to 3,5-di-tert-butylquinone (3,5-DTBQ) and prevents further oxidation or ring-opening reaction. In MeOH-MeCN (1 : 10) mixed solvent the complexes catalyze the oxidation of 3,5-DTBC to 3,5-DTBQ following Michaelis-Menten kinetics (*vide supra*). For this purpose, ~1 × 10^{-4} *M* solutions of the complexes were treated with a 100-fold concentrated solutions of 3,5-DTBC, under aerobic conditions at room

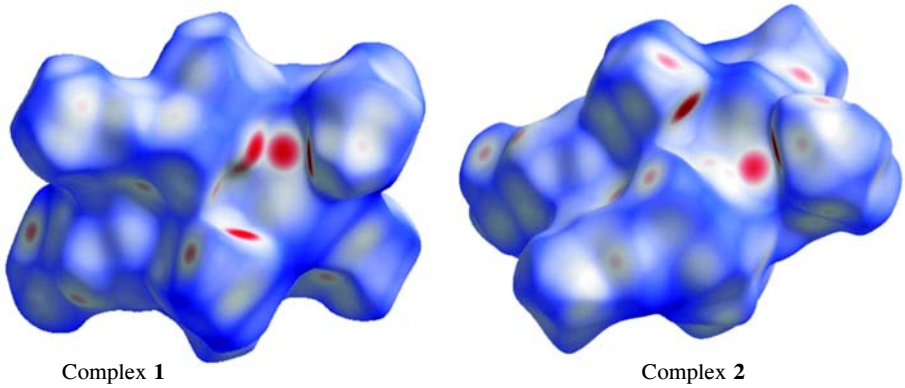

Complex **1** Complex **2**

Fig. 3. Hirshfeld surfaces mapped with d_{norm} for **1** (left) and **2** (right).

temperature and the course of the reaction was monitored by time dependent measurement of UV-Vis spectra up to 45 min. Spectral changes of complex **1** and **2** after addition of 3,5-DTBC are shown in Fig. 4. Addition of 3,5-DTBC causes a red shift in absorption band of complexes from 353 nm to 396 nm with a gradual increase of absorption intensity and this clearly indicates the formation of the corresponding quinone (3,5-DTBQ).

Kinetics for the formation of 3,5-DTBQ was followed by monitoring the growth of the absorbance at 396 nm in MeOH : MeCN (1 : 10). Solutions of $\sim 1 \times 10^{-4}$ *M* strength were treated with 3,5-DTBC (20, 30, 40, 50, 60, 70, 100 equivalents and 10, 20, 30, 40, 70, 80, 90, 100 equivalents for complexes **1** and **2**, respectively) and

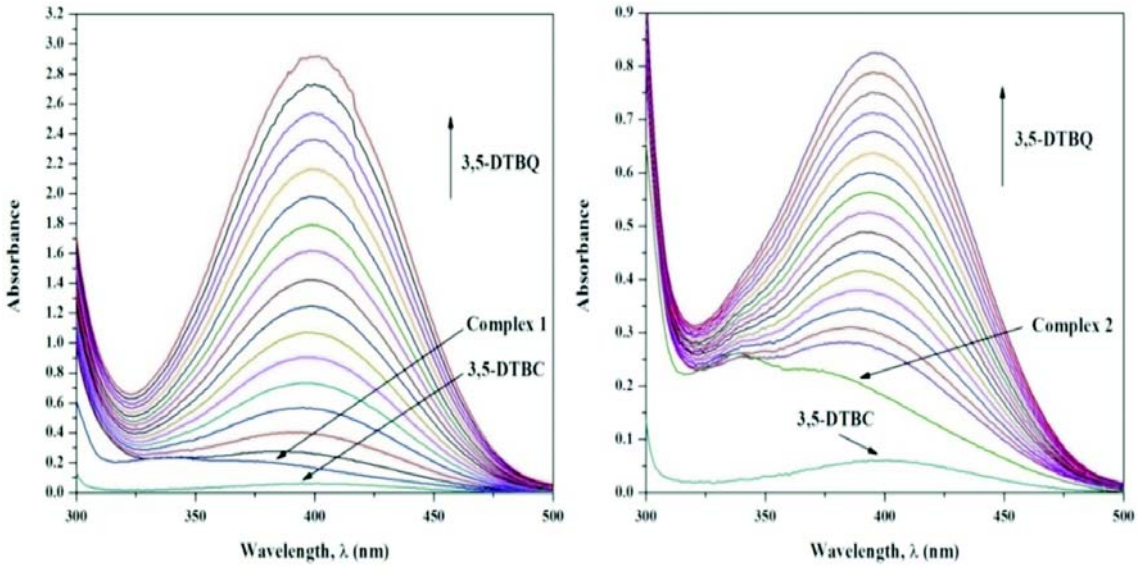

Complex **1** Complex **2**

Fig. 4. UV-Vis spectral changes for complexes **1** and **2** (conc. $\sim 1 \times 10^{-4}$ mol L^{-1}) upon addition of 100-fold 3,5-DTBC (conc. $\sim 1 \times 10^{-2}$ mol L^{-1}) in MeOH : MeCN (1 : 10) medium at 298 K at 3 min interval.

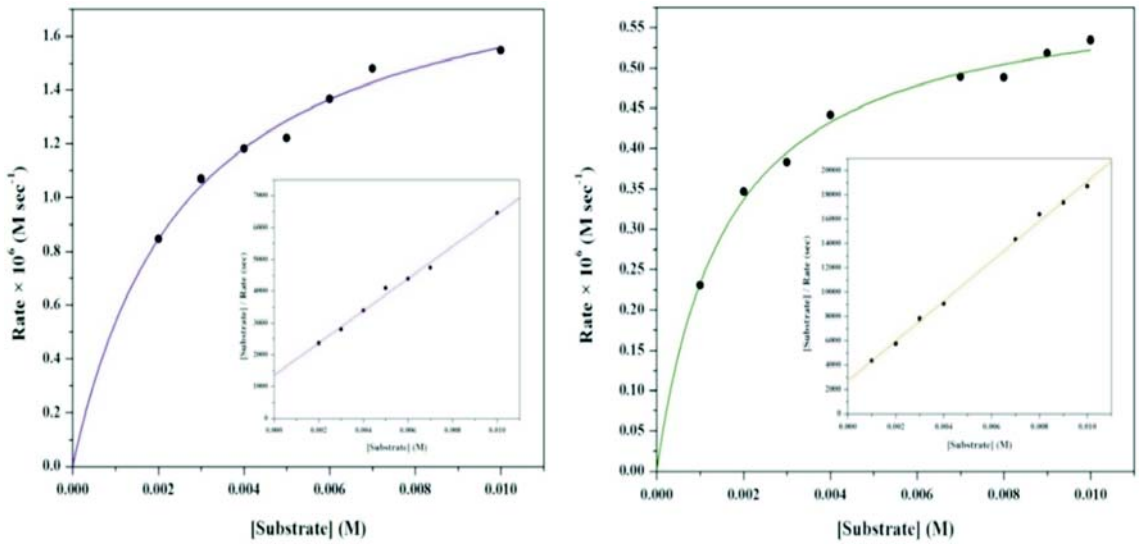

Complex **1** Complex **2**

Fig. 5. Plots of the initial rates versus substrate concentrations for the oxidation reaction catalyzed by **1** and **2**. The inset shows the Hanes-Woolf plot.

time scan was run for first 5 min of reaction (Fig. 5). The rates thus obtained were fitted by Michaelis-Menten approach and linearized by means of Hanes-Woolf plot of [S]/V vs [S] to calculate various kinetic parameters such as Michaelis-Menten constant (K_M) and the maximum reaction rate (V_{max}) achieved by the system at maximum (saturating) substrate concentration. The turnover numbers (k_{cat}) were calculated for the two complexes from the ratio of V_{max} values to the concentration of the corresponding complexes. The kinetic parameters V_{max}, K_M, and k_{cat} are listed in Table 3.

Table 3. Kinetic parameters

Complex	V_{max} (M s^{-1})	K_M (M)	k_{cat} (h^{-1})	k_{cat}/K_M (M^{-1} h^{-1})
1	1.975×10^{-6}	2.680×10^{-3}	71.089	26.526×10^{3}
2	6.092×10^{-7}	1.642×10^{-3}	21.931	13.356×10^{3}

The weakly coordinated ether oxygens are probably displaced by the deprotonated 3,5-DTBC to give the initial catalyst substrate adduct. From inspection of the kinetic data it is found that the k_{cat} value of **1** is more than three times than that of **2**. This difference in activity can be considered to have stemmed from the nature of the two trapped carboxylate anions. The measured pH values of the complexes in the mixed non-aqueous solvent medium have given some indication. Complex **1** has a pH ~12.38 while for complex **2** it is ~10.48 (the experimentally measured pH of MeOH/MeCN (1 : 10) is ~11.18)[21,22]. The higher solution pH of **1** as compared to **2** is attributable to the presence of uncoordinated $MeCOO^-$ in the former against $HCOO^-$ in the latter. A higher solution pH value favours the deprotonation of 3,5-DTBC more efficiently and stronger binding of the catecholate to the dicopper site. Therefore, the enhanced catalyst substrate interaction is believed to be responsible for **1** showing better catalytic activity than **2**.

The k_{cat} values of our complexes are similar to a number of other [Cu_2] complexes known in the literature (Table 4). Significantly higher value for $[Cu_2L_2(OH)]ClO_4$ is due to the presence of bridging hydroxido group between the two metal ions.

Table 4. Comparison of k_{cat} vaules of complexes **1-2** and other known phenoxido bridged Cu_2 complexes

Complex	Solvent	k_{cat} (h^{-1})	Ref.
$[Cu_2L_2(ClO_4)_2]$	MeOH	93.6	8
$[Cu_2L_2(OH)]ClO_4$	MeOH	233.4	8
$[Cu_2(L^1)_2(NCO)_2]$	MeOH	64	9
$[Cu_2(L^2)_2(NCO)_2]\cdot 2CH_3OH$	MeOH	98	9
$[(Cu\text{-}\mu\text{-}L_3)(CH_3COO)]_2$	MeOH	3.2	10
1	MeOH/MeCN (1 : 10)	71.0	Present work
2	MeOH/MeCN (1 : 10)	21.9	Present work

Conclusions

New [Cu_2] complexes, with weak ether oxygen coordination and having Cu···Cu separations in the range of 3.043–3.053 Å were found to be suitable for binding of catechol for its catalytic oxidation. The ether oxygen atoms of the ligand backbone provided longer Cu-O *apical* bonds in 2.41–2.49 Å range. Weak ether oxygen coordination thus gave elongated square pyramidal coordination geometry around each copper(II) ions. On Hirshfeld surfaces the hydrogen bonding interactions (O-H···O and N-H···O) responsible for trapping of acetate and formate anions were clearly observed as large deep red depressions. The cationic complexes did not show any type of coordination by available carboxylate anions, instead they were shown to be trapped by long ether-alcohol arms through hydrogen bonding. These carboxylate groups were thus unavailable for any higher order aggregation such as [Cu_4] or [Cu_6]. The new [Cu_2] systems in solution showed evidence of oxidation of catechol to quinone and can act as a catalyst in catechol oxidation reaction in spite of having double phenoxido bridges. Complex **1** showed higher catecholase activity as compared to **2** although both have similar structures of the dicopper unit. pH measurements in mixed non-aqueous solvent revealed that the solution of **1** had a higher pH value than that of **2** due to the presence of free $MeCOO^-$ ions in **1** as compared to $HCOO^-$ ions in **2**. The higher pH facilitates the deprotonation of catechol and hence its coordination to the metal centers resulting in the higher catecholase activity of complex **1**.

Acknowledgement

TSM is thankful to the University Grants Commission, New Delhi, India for the research fellowship. KC

thanks the Council of Scientific and Industrial Research, New Delhi, for her fellowship. DB and MD acknowledges IIT Kharagpur for the research fellowship. The authors also thank DST, New Delhi for the Single Crystal X-ray Diffractometer facility in the Department of Chemistry, IIT Kharagpur under its FIST program.

Supplementary data

Crystallographic data of the complexes have been deposited with the Cambridge Crystallographic Data Center with the CCDC numbers 1431950 (**1**) and 1431951 (**2**).

References

1. (a) A. R. Paital, T. Mitra, D. Ray, W. T. Wong, J. Ribas-Ariño, J. J. Novoa, J. Ribas and G. Aromí, *Chem. Commun.*, 2005, 5172; (b) D. Venegas-Yazigi, D. Aravena, E. Spodine, E. Ruiz and S. Alvarez, *Coord. Chem. Rev.*, 2010, **254**, 2086; (c) M. Pait, E. Colacio and D. Ray, *Polyhedron*, 2015, **88**, 90; (d) P. K. Nanda, V. Bertolasi, G. Aromí and D. Ray, *Polyhedron*, 2009, **28**, 987.
2. (a) S. Thyagarajan, N. N. Murthy, A. A. N. Sarjeant, K. D. Karlin and S. E. Rokita, *J. Am. Chem. Soc.*, 2006, **128**, 7003; (b) T. Jany, A. Moreth, C. Gruschka, A. Sischka, A. Spiering, M. Dieding, Y. Wang, S. H. Samo, A. Stammler, H. Bögge, G. Fischer von Mollard, D. Anselmetti and T. Glaser, *Inorg. Chem.*, 2015, **54**, 2679.
3. (a) R. E. H. M. B. Osório, R. A. Peralta, A. J. Bortoluzzi, V. R. De Almeida, B. Szpoganicz, F. L. Fischer, H. Terenzi, A. S. Mangrich, K. M. Mantovani, D. E. C. Ferreira, W. R. Rocha, W. Haase, Z. Tomkowicz, A. D. Anjos and A. Neves, *Inorg. Chem.*, 2012, **51**, 1569; (b) A. Biswas, L. K. Das, M. G. B. Drew, G. Aromí, P. Gamez and A. Ghosh, *Inorg. Chem.*, 2012, **51**, 7993.
4. (a) M. Sarkar, R. Clérac, C. Mathonière, N. G. R. Hearns, V. Bertolasi and D. Ray, *Inorg. Chem.*, 2010, **49**, 6575; (b) M. Sarkar, R. Clérac, C. Mathonière, N. G. R. Hearns, V. Bertolasi and D. Ray, *Inorg. Chem.*, 2011, **50**, 3922; (c) A. K. Ghosh, R. Clérac, C. Mathonière and D. Ray, *Polyhedron*, 2013, **54**, 196; (d) A. R. Paital, V. Bertolasi, G. Aromí, J. Ribas-Ariño and D. Ray, *Dalton Trans.*, 2008, **7**, 861.
5. (a) M. Sarkar, G. Aromí, J. Cano, V. Bertolasi and D. Ray, *Chem. Eur. J.*, 2010, **16**, 13825; (b) A. K. Ghosh, M. Pait, M. Shatruk, V. Bertolasi and D. Ray, *Dalton Trans.*, 2014, **43**, 1970.
6. (a) M. Pait, M. Shatruk, J. Lengyel, S. Gómez-Coca, A. Bauzá, A. Frontera, V. Bertolasi and D. Ray, *Dalton Trans.*, 2015, **44**, 6107; (b) A. K. Ghosh, M. Pait, R. Clérac, C. Mathonière, V. Bertolasi, A. Bauzá, A. Frontera, K. Pramanik and D. Ray, *Dalton Trans.*, 2014, **43**, 4076.
7. (a) K. S. Banu, T. Chattopadhyay, A. Banerjee, S. Bhattacharya, E. Suresh, M. Nethaji, E. Zangrando and D. Das, *Inorg. Chem.*, 2008, **47**, 7083; (b) I. A. Koval, P. Gamez, C. Belle, K. Selmeczi and J. Reedijk, *Chem. Soc. Rev.*, 2006, **35**, 814.
8. A. Biswas, L. K. Das, M. G. B. Drew, C. Diaz and A. Ghosh, *Inorg. Chem.*, 2012, **51**, 10111.
9. A. Biswas, L. K. Das and A. Ghosh, *Polyhedron*, 2013, **61**, 253.
10. V. K. Bhardwaj, N. Aliaga-Alcalde, M. Corbella and G. Hundal, *Inorg. Chim. Acta*, 2010, **363**, 97.
11. (a) N. Oishi, Y. Nishida, K. Ida and S. Kida, *Bull. Chem. Soc. Jpn.*, 1980, **53**, 2847; (b) J. Mukherjee and R. Mukherjee, *Inorg. Chim. Acta*, 2002, **337**, 429; (c) J. Mukherjee and R. Mukherjee, *Inorg. Chim. Acta*, 2002, **337**, 429; (d) F. Zippel, F. Ahlers, R. Werner, W. Haase, H. F. Nolting and B. Krebs, *Inorg. Chem.*, 1996, **35**, 3409; (e) C. H. Kao, H. H. Wei, Y. H. Liu, G. H. Lee, Y. Wang and C. J. J. Lee, *Inorg. Biochem.*, 2001, **84**, 171; (f) R. Wegner, M. Gottschaldt, H. Gorls, E. G. Jager and D. Klemm, *Chem. Eur. J.*, 2001, **7**, 2143; (g) M. Kodera, T. Kawata, K. Kano, Y. Tachi, S. Itoh and S. Kojo, *Bull. Chem. Soc. Jpn.*, 2003, **76**, 1957.
12. T. Shiga, N. Hoshino, M. Nakano, H. Nojiri and H. Oshio, *Inorg. Chim. Acta*, 2008, **361**, 4113.
13. R. R. Gagne, C. L. Spiro, T. J. Smith, C. A. Hamann, W. R. Thies and A. K. Shiemke, *J. Am. Chem. Soc.*, 1981, **103**, 4073.
14. G. J. Colpas, B. J. Hamstra, J. W. Kampf and V. L. Pecoraro, *Inorg. Chem.*, 1994, **33**, 4669.
15. S. K. Wolff, D. J. Grimwood, J. J. McKinnon, M. J. Turner, D. Jayatilaka and M. A. Spackman, Crystal Explorer 3.1, University of Western Australia, 2012.
16. Saint, Smart and XPREP, Siemens Analytical X-ray Instruments Inc., Madison, WI, 1995.
17. G. M. Sheldrick, SADABS, Software for Empirical Absorption Correction, University of Göttingen, Institute fur Anorganische Chemieder Universitat, Göttingen, Germany, 1999-2003.
18. G. M. Sheldrick, SHELXS-97, University of Göttingen, Göttingen, Germany, 1997.
19. G. M. Sheldrick, SHELXL-97, Program for Crystal Structure Refinement, University of Göttingen, Göttingen, Germany, 1997.
20. WinGX System, v. 1.80.05, L. Farrugia, University of Glasgow, UK.
21. D. Himmel, S. K. Goll, I. Leito and I. Krossing, *Angew. Chem., Int. Ed.*, 2010, **49**, 6885.
22. D. Himmel, S. K. Goll, I. Leito and I. Krossing, *Chem. Eur. J.*, 2011, **17**, 5808.

1948